Chinese Chemical Letters 32 (2021) 2459–2462

Contents lists available at ScienceDirect

Chinese Chemical Letters

journal homepage: www.elsevier.com/locate/cclet

Communication

Improving cycling stability of Bi-encapsulated carbon fibers for lithium/sodium-ion batteries by Fe_2O_3 pinning

Tianyi Hou[a], Anran Fan[a], Xiaohong Sun[a,*], Xi Zhang[a], Zhongkai Xu[a], Shu Cai[a], Chunming Zheng[b,*]

[a] School of Materials Science and Engineering, Key Laboratory of Advanced Ceramics and Machining Technology of Ministry of Education, Tianjin University, Tianjin 300072, China
[b] School of Chemistry and Chemical Engineering, State Key Laboratory of Hollow-Fiber Membrane Materials and Membrane Processes, Tiangong University, Tianjin 300387, China

ARTICLE INFO

Article history:
Received 26 November 2020
Received in revised form 12 January 2021
Accepted 28 January 2021
Available online 2 February 2021

Keywords:
Bismuth
Iron oxide
Pinning effect
Lithium-ion batteries
Sodium-ion batteries

ABSTRACT

Bi draws increasing attention as anode materials for lithium-ion batteries and sodium-ion batteries due to its unique layered crystal structure, which is in favor of achieving fast ionic diffusion kinetics during cycling. However, the dramatic volume expansion upon lithiation/sodiation and an insufficient theoretical capacity of Bi greatly hinder its practical application. Herein, we report the Fe_2O_3 nanoparticle-pinning Bi-encapsulated carbon fiber composites through the electrospinning technique. The introduction of Fe_2O_3 nanoparticles can prevent the growth and aggregation of Bi nanoparticles during synthetic and cycling processes, respectively. Fe_2O_3 with high specific capacity also contributes to the specific capacity of the composites. Consequently, the as-prepared Bi-Fe_2O_3/carbon fiber composite exhibits outstanding long-term stability, which delivers reversible capacities 504 and 175 mAh/g after 1000 cycles at 1 A/g for lithium-ion and sodium-ion batteries, respectively.

Lithium-ion batteries (LIBs) and sodium-ion batteries (SIBs) have attracted extensive attention in the field of high energy-density storage and the large-scale grid application, respectively [1–3]. Due to the abundant sodium resources, SIBs with price advantages and similar working principles are considered to be a promising counterpart of LIBs [4–7]. However, it remains a great challenge to find suitable anode materials for LIBs and SIBs with satisfied electrochemical performance beyond carbonaceous materials with limited capacities [8–10]. Transition-metal chalcogenides (TMCs) powered by conversion reactions can deliver high capacities [11,12]. Even so, TMCs always suffer from inadequate electronic conductivity and severe volume expansion and thus are subjected to poor cycling stability [13]. Alloying anode materials (*e.g.*, Sn, Sb) with high theoretical capacities and ideal voltage platforms are also promising candidates [14,15]. Thereinto, Bi has riveted increasing attention due to its high theoretical capacity of ~385 mAh/g and unique layered crystal structure with large lattice fringes along the *c*-axis ($d_{(003)}$ = 3.95 Å), which would allow fast ionic diffusion kinetics [16,17].

Though Bi has its unique merits, the theoretical capacity of Bi is still limited when compared with other alloying anode materials, such as Si (~4200 mAh/g) for LIBs and P (~2600 mAh/g) for SIBs [18,19]. However, severe volume expansion comes with high capacities. Compare with Si (~400%) and P (~440%), Bi shows a relatively smaller volume expansion of ~244% [19–21]. Nevertheless, the dramatic volume variation of Bi upon alloying and dealloying processes is still deleterious to cycling stability [19]. In order to address the poor cyclability of Bi anodes, many efforts have been made. Thereinto, encapsulating Bi nanoparticles into carbon architectures is reckoned as an effective strategy, where carbon matrix can accommodate the volume expansion of Bi nanoparticles, preventing structural failure [19]. For example, Hong *et al.* reported a spongiform porous Bi/C composite, which delivered a specific capacity of 380 mAh/g at 0.5 A/g after 500 cycles for LIBs [22]. Zhang *et al.* confined Bi nanodots in MOF-derived carbon arrays on carbon fiber cloth, and this composite achieved a stable lifespan up to 500 cycles for SIBs [23]. However, Bi-based anode materials still suffer from unsatisfied cyclability because of the aggregation of Bi nanoparticles during cycling and deliver insufficient capacities [24]. Hence, it is necessary to

* Corresponding authors.
E-mail addresses: sunxh@tju.edu.cn (X. Sun), zhengchunming@tiangong.edu.cn (C. Zheng).

https://doi.org/10.1016/j.cclet.2021.01.049

propose new strategies to further mitigate the volume expansion and impede the aggregation of Bi nanoparticles, and elevate the specific capacity of Bi-based anode composites to meet practical needs, simultaneously.

Herein, we prepared the Fe_2O_3 nanoparticle-pinning Bi-encapsulated carbon fiber composites through the electrospinning technique. Fe_2O_3 nanoparticles are *in-situ* formed in carbon fibers and prevent Bi nanoparticles from further growing and aggregating during synthetic and cycling processes, which is similar to the pinning effect for restricting the grain growth of the second-phase particles [25,26]. Similarly, Wang *et al.* employed TiO_2 nanoparticles to achieve physical pinning to stabilize SnS_2 on reduced graphene oxide [27]. Moreover, the Fe_2O_3 was introduced with another purpose, which is to take advantage of its high theoretical capacity (~1007 mAh/g) to compensate for the insufficient specific capacity of Bi [28]. In this work, the content of Bi and Fe_2O_3 in the composites was also investigated by adjusting the proportion of $Bi(NO_3)_3$ and $Fe(NO_3)_3$ with different Bi/Fe molar ratios of 2:1, 1:1 and 1:2, which are denoted as BFC-1, BFC-2 and BFC-3, respectively. Thereinto, BFC-2 exhibits the best electrochemical performance, delivering high reversible capacities of 504 and 175 mAh/g after 1000 cycles at 1 A/g for LIBs and SIBs, respectively.

Fig. 1a shows the X-ray diffraction (XRD) patterns of BFC-1, BFC-2, BFC-3 and Bi/carbon fibers (Bi/C). Most of the diffraction peaks of BFC composites can be indexed to the hexagonal Bi (JCPDS No. 85-1329). Meanwhile, except for the Bi phase, other diffraction peaks can be assigned to the cubic Fe_2O_3 (JCPDS No. 02-1047), and the intensity of Fe_2O_3 peaks gradually mounts up as the Fe_2O_3 content increases. The X-ray photoelectron spectroscopy (XPS) was employed to reveal the chemical state of BFC composites, and their XPS survey spectra are shown in Fig. S1 (Supporting information). In Fig. 1b, high-resolution XPS spectra of Bi 4f present two peaks at 164.2 and 158.9 eV for BFC-1, corresponding to Bi $4f_{5/2}$ and Bi $4f_{7/2}$, respectively [29]. As the Fe_2O_3 content increases, the peaks of Bi $4f_{5/2}$ and Bi $4f_{7/2}$ shift to 164.5 and 159.2 eV, which may account for the charge transfer from Bi to adjacent Fe_2O_3 [30], suggesting more obvious interaction between Bi and Fe_2O_3 nanoparticles in BFC-2 and BFC-3. Fig. 1c shows Fe $2p_{3/2}$ and Fe $2p_{1/2}$ doublets centered at 711.3 and 725.1 eV, indicating the presence of the Fe_2O_3 phase [28]. The left shift of Bi-O bonds shown in Fig. 1d corresponds to the XPS spectra of Bi.

Fig. 2a presents the network structure of BFC-2, which is composed of uniformed one-dimensional carbon fibers with a

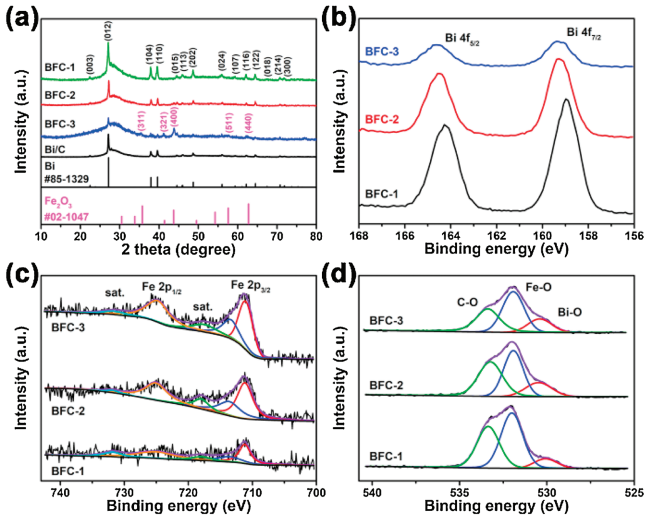

Fig. 1. (a) XRD patterns of the BFC-1, BFC-2, BFC-3 and Bi/C. High-resolution (b) Bi 4f, (c) Fe 2p, and (d) O 1s XPS spectra of the BFC-1, BFC-2 and BFC-3.

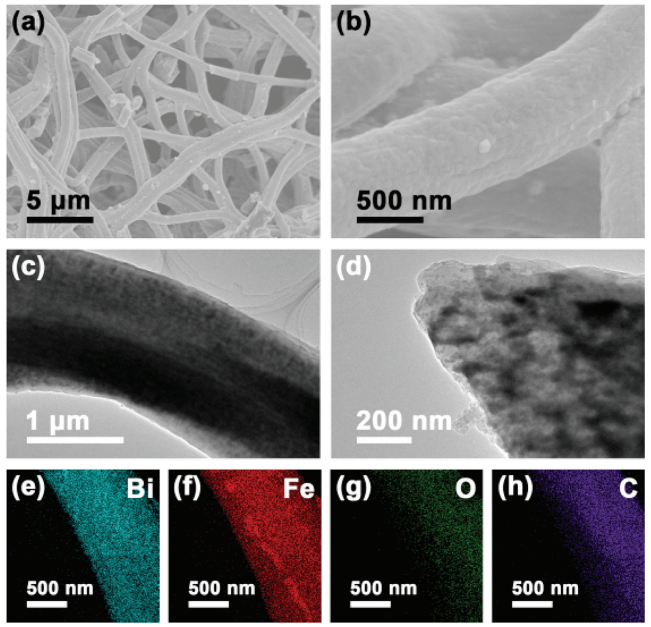

Fig. 2. (a,b) SEM, (c,d) TEM images and (e-h) the corresponding elemental mapping of Bi, Fe, O and C of BFC-2.

diameter of approximately 700 nm (Fig. 2b). The nanofibers are curly and pliable like noodles, and the outer surface is smooth without obvious particles, which indicates that the Bi and Fe_2O_3 nanoparticles have been mostly encapsulated into the carbon fibers without exposure. Scanning electron microscopy (SEM) images of BFC-1, BFC-3 and Bi/C show similar network structures compared with BFC-2 (Fig. S2 in Supporting information). The Bi/Fe molar ratios of BFC-1, BFC-2 and BFC-3 are determined to be 1.64, 0.81 and 0.41 from energy dispersive spectroscopy (EDS) results (Fig. S3 in Supporting information), giving theoretical capacities of around 503, 584 and 685 mAh/g based on the Bi-Fe_2O_3 system, respectively. The deviation of the Bi/Fe ratios between as-prepared BFC samples from their precursor solutions is because the low melting point of the Bi metal (~271.5 °C) causes the loss of the Bi content of BFC composites during calcination. The contents of Bi, Fe_2O_3 and C in as-prepared samples can be further quantified by combining thermogravimetric analysis (TGA, Fig. S4 in Supporting information) and summarized in Table S1 (Supporting information). Detailed microstructures of BFC-2 are revealed by transmission electron microscopy (TEM), where Bi and Fe_2O_3 nanoparticles are uniformly distributed in the carbon fiber (Figs. 2c and d). EDS mapping images from the STEM dark-field image (Fig. S5 in Supporting information) present the elemental distribution of Bi, Fe, O and C, further demonstrating the homogeneous distribution of Bi and Fe_2O_3 in carbon fiber (Figs. 2e–h).

The electrochemical performance of the as-prepared samples was evaluated in Li and Na half cells. Fig. 3a shows the cycling performance of the BFC-1, BFC-2, BFC-3 and Bi/C in Li half cells at a current density of 0.1 A/g. BFC-2 exhibits a high reversible capacity of 564 mAh/g over 50 cycles, while BFC-1, BFC-3 and Bi/C only maintain lower capacities of 445, 400 and 274 mAh/g (Fig. S6 in Supporting information). Compared with BFC-2, the inferior performance of BFC-1 may be contributed to the slight capacity contribution and inadequate restriction effect of the low Fe_2O_3 content. However, as the Fe_2O_3 content increases, BFC-3 also suffers from the severe volume expansion of Fe_2O_3. Hence, Bi and Fe_2O_3 nanoparticles can confine each other during cycling to achieve good stability. As shown in the cyclic voltammetry (CV)

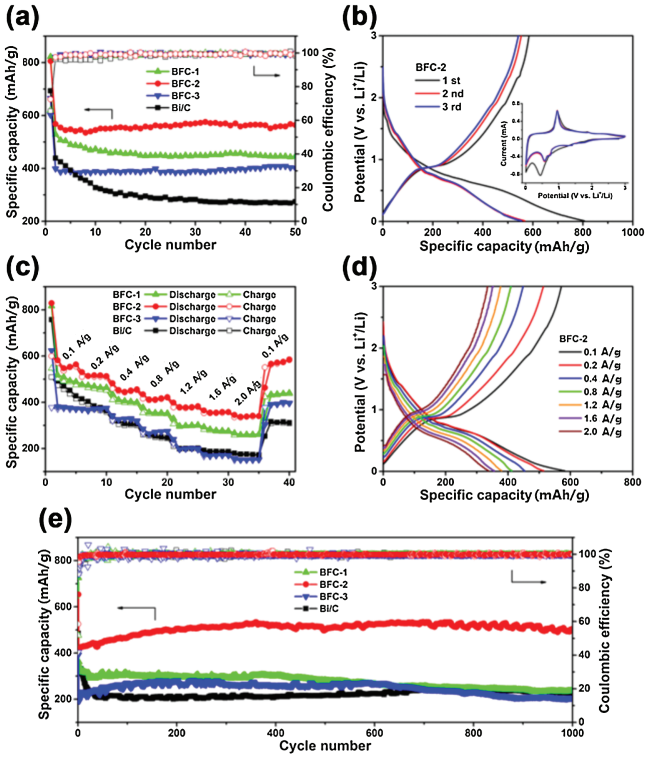

Fig. 3. Lithium storage properties of the BFC-1, BFC-2, BFC-3 and Bi/C. (a) Cycling performance at 0.1 A/g. (b) Galvanostatic charge-discharge and CV curves of BFC-2 in initial three cycles. (c) Rate capability and (d) charge-discharge curves at various current densities of the BFC-2. (e) Long-term stability at 1 A/g.

curves of BFC-2 (Fig. 3b), a strong reduction peak centered at ~0.45 V in the first scan can be attributed to the formation of solid electrolyte interface (SEI) films, alloying processes of Bi, and the conversion reaction of Fe_2O_3 [31,32]. In the following two scans, two cathodic peaks at around 0.6 and 0.75 V can be attributed to the formation of LiBi and Li_3Bi [33]. The anodic peak at ~0.96 V is assigned to the de-alloying reaction of Li_3Bi [33]. Two weak redox pairs at around 1.4/1.8 V and 1.7/2.4 V may relate to the reduction and oxidation of a small amount of Bi^{3+} intermetallic Bi [34]. No obvious redox peaks of the conversion reaction of Fe_2O_3 can be seen, which probably overlap with that of the alloying reaction of Bi [32]. The obvious difference between the first and the following two scans is ascribed to the decomposition of electrolytes and the irreversible formation of SEI films, which is also accounted for the limited initial Coulombic efficiency if BFC-2 (72.5%) and the capacity loss in the first cycle as shown in its charge-discharge curves. Though this value is not satisfied, it still higher than that of Bi/C (69.2%, Fig. S7 in Supporting information), and the Coulombic efficiency of BFC-2 quickly increases to 97.5% in the second cycle, indicating the good electrochemical reversibility of BFC-2.

Due to the effective Fe_2O_3 pinning, BFC-2 presents excellent rate capability, delivering a reversible capacity of 338 mAh/g at 2 A/g, and when the current density returns to 0.1 A/g, a reversible capacity of 567 mAh/g can be retained (Fig. 3c). As the current density increases from 0.1 A/g to 2 A/g, the polarization voltage slightly increases from 0.4 V to 0.6 V, suggesting fast reaction kinetics of BFC-2 (Fig. 3d). Meanwhile, BFC-2 exhibits outstanding long-term stability (Fig. 3e). After 1000 cycles, BFC-2 can sustain a reversible capacity of 504 mAh/g at 1 A/g with the Coulombic efficiency of ~100% (Fig. S8 in Supporting information), which is much higher than that of BFC-1 (235 mAh/g), BFC-3 (206 mAh/g), and Bi/C (226 mAh/g). The capacity of BFC-1 decays continuously along with cycling, while the specific capacity of BFC-2 increases first during cycling and then remain stable with marginal capacity loss, which may be related to the introduction of an appropriate amount of Fe_2O_3 nanoparticles to BFC-2. According to previous research, this extra capacity as widely reported in transition-metal oxides for LIBs is most likely attributed to the reversible formation of a polymer or gel-like film on metallic nanograins [35] and the interfacial Li^+ storage between electrochemically reduced metal nanoparticles and Li_2O, accompanied by a large number of spin-polarized electrons stored in metallic nanoparticles [36]. To the best of our knowledge, the cycling performance of BFC-2 exceeds most of the previous work (Table S2 in Supporting information).

When tested in Na half cells, BFC-2 also shows good cycling stability, delivering a reversible capacity of 332 mAh/g at 0.1 A/g over 50 cycles (Fig. 4a and Fig. S9 in Supporting information). As shown in the CV curves of BFC-2 (Fig. 4b), two pairs of redox peaks at around 0.43/0.73 and 0.61/0.83 V correspond to the formation and oxidation of NaBi and Na_3Bi [17], and a pair of broad cathodic/anodic peak at about 0.8/1.4 V is attributed to the conversion reaction of Fe_2O_3 [28,37]. BFC-2 shows an initial discharge capacity of 538 mAh/g with a Coulombic efficiency of ~70%, which is caused by the decomposition of electrolytes to form SEI films in the first cycle. Though the Coulombic efficiency of BFC-2 in the initial cycle is slightly lower than that of Bi/C (74%, Fig. S10 in Supporting information), it quickly goes up to 96.8% in the second cycle owing to the effectiveness of carbon encapsulating and Fe_2O_3 pinning. BFC-2 possesses decent rate capability for SIBs (Fig. 4c), showing a reversible capacity of 203 mAh/g at 2 A/g (Fig. 4d), which is around twice that of BFC-1 (91 mAh/g) and BFC-3 (102 mAh/g), and more than three times that of Bi/C (58 mAh/g). Moreover, Fig. 4e exhibits the long-term stability of these as-prepared samples, where BFC-2 keeps stable up to 1000 cycles with a reversible capacity of 175 mAh/g at 1 A/g (Fig. S11 in Supporting information). Compared with previous reports, BFC-2 still presents decent and well-

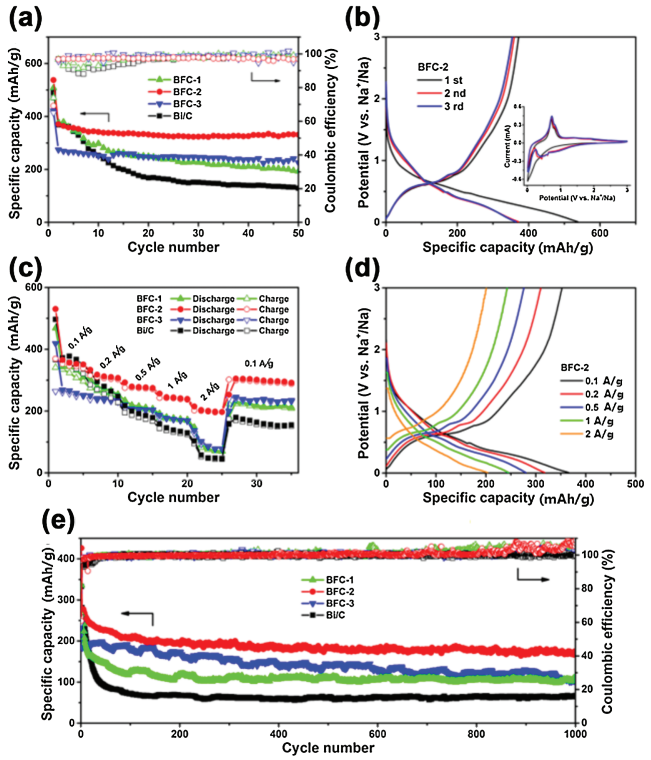

Fig. 4. Sodium storage properties of the BFC-1, BFC-2, BFC-3 and Bi/C. (a) Cycling performance at 0.1 A/g. (b) Galvanostatic charge-discharge and CV curves of BFC-2 in initial three cycles. (c) Rate capability and (d) charge-discharge curves at various current densities of the BFC-2. (e) Long-term stability at 1 A/g.

matched cycling performance as shown in Table S3 (Supporting information).

The impedance difference between BFC-2 and Bi/C were investigated by electrochemical impedance spectroscopy (EIS) measurements. As shown in the Nyquist plots (Fig. S12 in Supporting information), compared with Bi/C, BFC-2 possesses smaller solution resistance (R_s) and charge-transfer resistance (R_{ct}) after 50 cycles in Li and Na half cells (Table S4 in Supporting information), which means the facile ionic diffusion of Bi and Fe_2O_3 nanoparticles in BFC-2 enabled by the pinning effect leading to easier charge transfer kinetics [6,9] and indicates the formation of stable SEI films [38]. Owing to this kinetic advantage, the loading of active materials shows little negative effects on the performance of BFC-2 electrodes. Even at an active material loading of ~2.6 mg/cm^2, BFC-2 still possesses reversible capacities of 531 and 304 mAh/g at 100 mA/g after 15 cycles in Li half cells and 30 cycles in Na half cells, respectively (Fig. S13 in Supporting information), corresponding to 97% and 94% capacity retention compared with its specific capacities of ~1 mg/cm^2 electrodes for LIBs and SIBs. In contrast, Bi/C only holds 86% and 56% capacity retention for lithium and sodium storage, respectively (Fig. S14 in Supporting information). This suggests BFC-2 has great potential for practical applications in LIBs and SIBs. Meanwhile, the cut-off voltage has a small effect on the electrochemical activity of BFC-2 electrodes. The charge-discharge curves of BFC-2 cycled between 0.01–2 V coincide well with that of BFC-2 with an upper cut-off voltage of 3 V (Fig. S15 in Supporting information). However, Bi/C is subjected to obvious capacity loss between 0.01 V and 2 V in Na half cells, which may be accounted for the poor reversibility of alloying reaction of Bi and aggregation of Bi nanoparticles during cycling [24].

In order to demonstrate the pinning effect of Fe_2O_3 nanoparticles, SEM and TEM were used to examine post-cycling BFC-2 and Bi/C electrodes. Fig. S16 (Supporting information) shows the structural degradation of Bi/C in Li and Na half cells. The surface of Bi/C fibers becomes rough and uneven after cycling in Li half cells, indicating the aggregation of Bi nanoparticles or even the leakage of Bi from the carbon matrix. In Na half cells, Bi/C fibers are cracking into nanoparticles after cycling, leading to poor cycling performance of Bi/C, which can be accounted for the severe volume expansion of Bi nanoparticles. In contrast, BFC-2 can maintain its original structure both in Li and Na half cells (Fig. S17 in Supporting information). The good structural stability of BFC-2, indicating that the introduction of Fe_2O_3 nanoparticles can confine the volume expansion of Bi nanoparticles. Meanwhile, due to the pinning effect, Bi and Fe_2O_3 nanoparticles can still distribute uniformly in carbon fibers after cycling (Fig. S18 in Supporting information). However, significant growth and aggregation of Bi nanoparticles are shown in TEM images of post-cycling Bi/C, causing the breakage of Bi/C fibers (Fig. S19 in Supporting information). The good structural maintenance of BFC-2 guarantees its good cyclability and demonstrates the effectiveness of the Fe_2O_3 pinning effect.

In conclusion, we propose a strategy to improve the cycling performance of Bi-based anode materials by introducing Fe_2O_3 pinning. The Fe_2O_3 nanoparticle-pinning Bi-encapsulated carbon fiber composites were prepared *via* electrospinning. Bi and Fe_2O_3 nanoparticles in carbon fibers can prevent each other from further aggregating during cycling, thus leading to cycling stability and rate capability. Meanwhile, the introduction of Fe_2O_3 is also beneficial for elevating the specific capacity of the composite. Hence, the optimized composite (BFC-2) presents outstanding long-term cycling stability and excellent rate capability, demonstrating itself as a potential anode material for LIBs and SIBs. Besides, this Fe_2O_3 nanoparticle-pinning strategy shows great promise in electrode design for rechargeable batteries.

Declaration of competing interest

The authors declare that they have no known competing financial interests or personal relationships that could have appeared to influence the work reported in this paper.

Acknowledgments

The authors acknowledge the financial support by the National Natural Science Foundation of China (NSFC, Nos. 52073212, 51772205, 51772208) and General Program of Municipal Natural Science Foundation of Tianjin (Nos. 17JCYBJC17000, 17JCYBJC22700).

Appendix A. Supplementary data

Supplementary material related to this article can be found, in the online version, at doi:https://doi.org/10.1016/j.cclet.2021.01.049.

References

[1] M. Armand, J.M. Tarascon, Nature 451 (2008) 652–657.
[2] H.L. Pan, Y.S. Hu, L.Q. Chen, Energy Environ. Sci. 6 (2013) 2338–2360.
[3] Y. Chen, X. Hu, B. Evanko, et al., Nano Energy 46 (2018) 117–127.
[4] Y. Chen, B. Wang, T. Hou, et al., Chin. Chem. Lett. 29 (2018) 187–190.
[5] J. Xu, W. Wei, X. Zhang, L. Liang, M. Xu, Chin. Chem. Lett. 30 (2019) 1341–1345.
[6] N. Zhang, X. Li, T. Hou, et al., Chin. Chem. Lett. 31 (2020) 1221–1225.
[7] J. Guo, X. Sun, K. Shen, et al., Chem. Eng. J. 393 (2020) 124703.
[8] Z. Zhang, Y. Hou, S. Zhang, et al., Chin. Chem. Lett. 29 (2018) 1656–1660.
[9] T. Hou, S. Yue, X. Sun, et al., Appl. Surf. Sci. 505 (2020) 144633.
[10] T. Hou, G. Tang, X. Sun, et al., RSC Adv. 7 (2017) 43636–43641.
[11] Q. Ren, N. Qin, B. Liu, et al., J. Mater. Chem. A 8 (2020) 3450–3458.
[12] B. Deng, L. Shen, Y. Liu, et al., Chin. Chem. Lett. 28 (2017) 2281–2284.
[13] Z. Ali, T. Zhang, M. Asif, et al., Mater. Today 35 (2020) 131–167.
[14] Y. Dong, Y. Feng, J. Deng, P. He, J. Ma, Chin. Chem. Lett. 31 (2020) 909–914.
[15] W. Wei, F.F. Jia, K.F. Wang, P. Qu, Chin. Chem. Lett. 28 (2017) 324–328.
[16] D.W. Su, S.X. Dou, G.X. Wang, Nano Energy 12 (2015) 88–95.
[17] P. Xue, N. Wang, Z. Fang, et al., Nano Lett. 19 (2019) 1998–2004.
[18] M.N. Obrovac, V.L. Chevrier, Chem. Rev. 114 (2014) 11444–11502.
[19] M. Lao, Y. Zhang, W. Luo, et al., Adv. Mater. 29 (2017) 1700622.
[20] J. Yang, Y.X. Wang, S.L. Chou, et al., Nano Energy 18 (2015) 133–142.
[21] J. Sun, H.W. Lee, M. Pasta, et al., Energy Storage Mater. 4 (2016) 130–136.
[22] W. Hong, A. Wang, L. Li, et al., Adv. Funct. Mater. 31 (2021) 2000756.
[23] Y. Zhang, Q. Su, W. Xu, et al., Adv. Sci. 6 (2019) 1900162.
[24] H. Yang, L.W. Chen, F. He, et al., Nano Lett. 20 (2020) 758–767.
[25] N. Fujiyama, T. Nishibata, A. Seki, et al., Sci. Technol. Adv. Mater. 18 (2017) 88–95.
[26] N. Maazi, Mater. Sci. Eng. A 528 (2011) 4994–5001.
[27] H.E. Wang, X. Zhao, X. Li, et al., J. Mater. Chem. A 5 (2017) 25056–25063.
[28] T. Hou, X. Sun, D. Xie, et al., Chem. Eur. J. 24 (2018) 14786–14793.
[29] W. Chai, W. Yin, K. Wang, et al., Electrochim. Acta 325 (2019) 134927.
[30] S. Mandal, C.K. Ghosh, D. Sarkar, U.N. Maiti, K.K. Chattopadhyay, Solid State Sci. 12 (2010) 1803–1808.
[31] H. Yin, Q. Li, M. Cao, et al., Nano Res. 10 (2017) 2156–2167.
[32] Z.G. Wu, Y.J. Zhong, J. Liu, et al., J. Mater. Chem. A 3 (2015) 10092–10099.
[33] Y. Zhong, B. Li, S. Li, et al., Nano-Micro Lett. 10 (2018) 56.
[34] H. Yuan, Y. Jin, X. Chen, et al., ACS Sustain. Chem. Eng. 7 (2019) 6033–6042.
[35] S. Laruelle, S. Grugeon, P. Poizot, et al., J. Electrochem. Soc. 149 (2002) A627–A634.
[36] Q. Li, H. Li, Q. Xia, et al., Nat. Mater. 20 (2021) 76–83.
[37] X.J. Liu, T.Q. Chen, H.P. Chu, et al., Electrochim. Acta 166 (2015) 12–16.
[38] Y. Jiang, Y. Li, P. Zhou, et al., Adv. Mater. 29 (2017) 1606499.